29th Congress of the International Council
of the Aeronautical Sciences
St. Petersburg, Russia; September 7–12, 2014

THE EFFECTS OF NONLINEARITY ON CROSSFLOW RECEPTIVITY

Christian Thomas[*] **, Philip Hall**[*] **, Christopher Davies**[**]
[*]**Imperial College London,** [**]**Cardiff University**

Keywords: *Boundary-layer, crossflow, nonlinearity, disturbance development, receptivity*

Abstract

Using a vorticity form of the Navier-Stokes equations the effects of nonlinearity on the development and receptivity of crossflow disturbances in the Swept Hiemenz boundary-layer are investigated. Steady perturbations are generated using wall suction and blowing that are distributed periodically as either a strip or point holes. The method, size and the location of the forcing are shown to significantly influence the receptivity of the crossflow within the boundary-layer. Perturbations excited by periodic blowing holes have considerably larger amplitudes than those generated by suction holes or strips. A linear log relationship is derived that relates the receptivity amplitude of the linear only disturbances with the chord position that the nonlinear primary Fourier perturbation attains a state of equilibrium: location that the maximum absolute amplitude of the primary disturbance shows distinct differences to the linear only solution. Further the size of the chordwise velocity perturbation at the location corresponding to equilibrium can be predicted directly from the linear only solutions. Thus, if the receptivity amplitude of the linear perturbation is smaller than some given threshold magnitude, nonlinear flow characteristics can be predicted directly from the computationally less expensive linear analysis.

1 Introduction

The current investigation concerns the development and receptivity of crossflow disturbances within the swept Hiemenz boundary-layer. Both the linear and nonlinear stages of the laminar-turbulent transition process are considered. The crossflow instability was examined by [1] and takes the form of stationary co-rotating vortices (and occasionally traveling disturbances). Gray [2] observed crossflow vortex structures on a swept wing, while in the context of a rotating disk and cone, stationary crossflow vortices have been observed by [3] and [4]. The linear, nonlinear and secondary instability stages of crossflow development and the laminar-turbulent transition mechanisms in the Swept Hiemenz flow were investigated by [5]. Their analysis was based on a system of nonlinear parabolized stability equations (NPSE). Detailed descriptions of the vortex development, inflectional velocity profiles and the generation of so-called half-mushroom structures were discussed. A high-frequency secondary instability was observed prior to the onset of transition, agreeing with the earlier experiments on a swept cylinder by [6] and swept wing by [7]

In regard to the initial properties of the flow system, environmental factors past a solid surface can filter into the boundary-layer, seeding steady and unsteady fluctuations of the undisturbed state. This process is known as boundary-layer receptivity and characterises the initial stages of the laminar-turbulent transition process [8]. External causes for receptivity and the laminar flow breakdown can be attributed to the flow interaction with freestream acoustics, turbulence, vortices and wall deformations, including surface curvature, discontinuities and roughness [9]. Receptivity of the boundary-layer establishes the initial conditions for the amplitude, frequency and phase of the disturbances in the flow. If the

initial amplitude of the perturbation remains relatively weak, the path to transition is driven by the excitation and development of a primary modal instability; crossflow vortex on swept surfaces. Modal growth of an initially small amplitude disturbance can be computed using linear stability theory, but as the magnitude of the crossflow instability grows, nonlinear processes arise through modal interaction with higher order harmonics. The magnitude of a disturbance is characterized by several initial flow properties, including the Reynolds number, spanwise periodicity and frequency. Further, the shape, location and size of the receptivity forcing, influences the amplitude of the disturbance and can significantly affect the onset of nonlinear effects and transition. Theoretical investigations concerning the receptivity of three-dimensional boundary-layers to wall roughness have been undertaken by [10], [11], [12] amongst many others.

Crossflow development and receptivity are investigated here using an extended scheme of the vorticity formulation derived by [13]. It is the aim of this study to characterise the effects of nonlinearity on the receptivity of crossflow disturbances and determine the differences (if any) with linear solutions.

2 Formulation

2.1 Base Flow and Perturbation Equations

Consider an incompressible viscous fluid in a Cartesian coordinate system $\mathbf{x}^* = \{x^*, y^*, z^*\}$ relative to a swept plate, where the three coordinates respectively denote the chordwise, spanwise and wall-normal directions. Uniform flow fields $U_\infty = mx^*$ and V_∞ are directed along the chord and spanwise axis, engineering the swept Hiemenz flow that impinges on an inclined plate. Units of length are scaled on the boundary-layer thickness $\delta = \sqrt{\nu/m}$ for ν the kinematic viscosity of the fluid. Corresponding velocity components are dimensionalized using the spanwise flow field V_∞.

The development of the crossflow instability in the swept Hiemenz boundary-layer is investigated using a vorticity form of the Navier-Stokes equations [13]. The total velocity and vorticity fields are given as

$$\mathbf{U} = \mathbf{U_B} + \bar{\mathbf{u}}, \quad \text{and} \quad \Omega = \Omega_B + \bar{\omega}, \qquad (1a)$$

where the undisturbed flow is defined as

$$\mathbf{U_B} = \left\{ \frac{x}{R} f'(z), g(z), -\frac{1}{R} f(z) \right\}. \qquad (1b)$$

and perturbation fields are denoted as

$$\bar{\mathbf{u}} = \{\bar{u}, \bar{v}, \bar{w}\}, \quad \text{and} \quad \bar{\omega} = \{\bar{\omega}_x, \bar{\omega}_y, \bar{\omega}_z\}. \quad (1c)$$

Functions f and g are dependent on the wall-normal direction and are calculated by solving the well-known Falker-Skan equations, while the Reynolds number

$$R = \frac{V_\infty \delta}{\nu}. \qquad (2)$$

A set of primary perturbation fields are defined as $\{\bar{\omega}_x, \bar{\omega}_y, \bar{w}\}$ where the governing system of equations are composed of the vorticity transport equation and Poisson relationship

$$\frac{\partial \bar{\omega}}{\partial t} + \nabla \wedge \{\Omega \wedge \mathbf{U}\} = \frac{1}{R} \nabla^2 \bar{\omega}, \qquad (3a)$$

$$\nabla^2 \bar{\mathbf{u}} + \nabla \wedge \bar{\omega} = 0. \qquad (3b)$$

The remaining secondary variables $\{\bar{u}_x, \bar{u}_y, \bar{\omega}\}$ are given by rearranging the definitions for vorticity and the solenoidal condition

$$\bar{\omega} = \nabla \wedge \bar{u} \quad \text{and} \quad \nabla \cdot \bar{\omega} = 0. \qquad (4)$$

Disturbances are assumed to be periodic along the spanwise y-direction. Hence, perturbations are represented using a truncated Fourier series as

$$q(\mathbf{x}, t) = \sum_{k=-N_y}^{N_y - 1} q_k(x, z, t) e^{ik\beta y}, \qquad (5)$$

where β is the spanwise wavenumber of the perturbation. Here k is the kth harmonic of the spanwise Fourier series (where $k = 1$ represents the primary disturbance) and N_y is an integer that represents half the number of modes in the series.

Disturbances are then expanded in terms of Chebyshev polynomials as

$$q_k(x,z,t) = \sum_{j=1}^{N_z} \hat{q}_{k,j}(x,t)T_j(\xi), \qquad (6)$$

where T_j is the jth Chebyshev polynomial. Here N_z is the order of the series truncation and j is an odd and even integer for the respective primary and secondary variables. The system of governing equations (3) are then integrated twice with respect to the mapped variable ξ, generating a simple set of banded matrix representations for the wall-normal variation. Finally, chordwise derivatives are represented using a fourth-order centred, compact finite difference approximation and the time-marching is treated using a combination of a predictor-corrector scheme and semi-implicit methods.

2.2 Excitation of the Disturbances

Steady perturbations are established by exciting the undisturbed flow using wall suction or blowing

$$\bar{u} = \bar{v} = 0 \quad \text{and} \quad \bar{w} = \bar{w}_w(x,y,t) \quad \text{on} \quad z = 0. \qquad (7a,b,c)$$

The function $\bar{w}_w$ is chosen to be both periodic along the spanwise direction and in time, so as to excite the desired stationary or travelling crossflow disturbance:

$$\bar{w}_w = \sum_{k=-N_y}^{N_y-1} w_{k,w}h(x)e^{i(k\beta y - \omega t)}, \qquad (8a)$$

where ω is the frequency of forcing, $w_{k,w}$ specifies the magnitude of the kth Fourier mode and the chord distribution $h = h(x)$ is described as a normalized Gaussian function

$$h(x) = \frac{1}{\sqrt{2\pi}}e^{-(x-x_f)^2/2}, \qquad (8b)$$

for x_f the centre of the wall forcing.

Suction and/or blowing are generated using two methods characterized by the Fourier amplitudes:

I. $w_{1,w} = c$ and $w_{k,w} = 0 \quad \forall \quad k \neq 1$ and

II. $w_{k,w} = c \quad \forall \quad k \neq 1$.

Scheme **I** corresponds to a periodic suction/blowing strip, where the sign of c has no effect on the receptivity of the disturbance. Only the primary mode is excited. However, through nonlinear interaction the growth of the higher order harmonics is established. For method **II** all of the harmonics are forced equally, representing a band of periodic holes prescribed with either suction (negative c) or blowing only (positive c). The size of the amplitude c then imposes conditions on the receptivity analysis.

3 Results

3.1 Definitions

In parabolized stability equation analysis of the linear development of crossflow (such as that carried out by [5]), it is assumed that crossflow can be defined in the form

$$q(\mathbf{x},t) = A_c \tilde{q}(x,z)e^{\int_{x_0}^x \alpha(x')dx' + i\{\beta y - \omega t\}}, \qquad (9)$$

where $\tilde{q}$ is a shape function that varies slowly along the chord direction, α is the chord wavenumber of the perturbation and x_0 defines the location for neutral stability (about $x \sim 186$ for crossflow). The constant parameter A_c represents the magnitude of the disturbance, which is described herein as the receptivity amplitude. For linear analysis the receptivity amplitude is directly proportional to the size of the initial forcing c as

$$A_c = cA_1$$

where A_1 is the receptivity amplitude of the disturbance when $c = 1$.

Neglecting the slow chordwise variation of the shape function $\tilde{q}$ in equation (9), the definition for linear crossflow can be simplified further, so that disturbances are given as

$$q(\mathbf{x},t) \approx A_c \tilde{q}(z)e^{\int_{x_0}^x \alpha(x')dx' + i\{\beta y - \omega t\}}. \qquad (10)$$

Replacing the function q with the primary Fourier perturbation field u_1 and setting the respective maximum absolute amplitude as
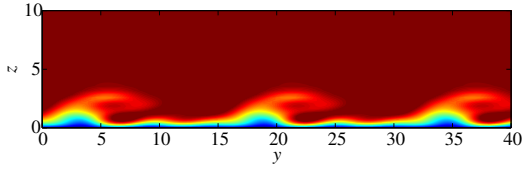
$$M(x) = \max_z |u_1(x,z)|, \qquad (11)$$

Fig. 1 Total chordwise velocity in the (y, z)-plane at $x = 450$ for $\beta = 0.4$ and $R = 500$.

the definition for the linear receptivity amplitude

$$A_c = \frac{M(x)}{\left| e^{\int_{x_0}^{x} \alpha(x) dx} \right|}, \qquad (12)$$

where it is assumed that $|\tilde{u}_1(z)| = 1$. For a prescribed set of initial flow conditions the exponential denominator is a constant function in x and is independent of the choice of wall forcing. Thus, once M is known, it is a relatively simple task to compute the receptivity amplitude A_c. Further, applying the above definitions to the solutions of the nonlinear investigation generates the equivalent nonlinear receptivity amplitudes.

3.2 Disturbance Development

A steady stationary crossflow disturbance is established for the initial flow conditions $R = 500$ and $\beta = 0.4$. A crossflow disturbance is generated using the wall forcing scheme **I**, which is prescribed about the chord location $x_f = 186$ with amplitude $c = 0.01$. The periodic suction/blowing strip is switched on at time $t = 0$ and excites disturbances within the boundary-layer. Downstream of the forcing the perturbation evolves, marching downstream along the chordwise direction. Eventually a steady crossflow vortex forms and nonlinear characteristics are attained. The number of Chebyshev polynomials N_z used along the wall-normal direction was set to 48, while only $N_y = 4$ spanwise Fourier modes were used in all subsequent analysis. Indeed it was suggested by [5] that the nonlinear characteristics of the crossflow vortex could be modeled successfully using only the primary Fourier mode and its zeroth and second order harmonics.

Figure 1 depicts a (y, z)-plane cut of the total chordwise U-velocity, plotted using colour contours at the chord location $x = 450$. The flow dynamics are plotted over two spanwise wavelengths and the scale along both the spanwise and wall-normal directions are equal to illustrate the genuine flat shape of the fully developed crossflow disturbance. Contours are plotted from a value of zero (blue colour) near the wall through to a maximum magnitude of approximately 0.9 (red colour) in the far-field. The Crossflow vortices are found to evolve into shapes described by [5] as half-mushroom structures. At the chord location shown, the nonlinear effects have emerged and the disturbance has rolled into vortices, creating regions of low and high velocity. This in turn results in significant variations in the boundary-layer thickness along the span.

3.3 Absolute Velocity

Figure 2 displays several results of the maximum amplitude of the primary Fourier component of the $\bar{u}$-velocity against the chordwise x-direction. The expression for M, equation (11), is again utilised to simplify all subsequent notation. A semi-log scale has been used along the vertical axis to assist visualization, while the parameter M has been normalized using the factor $R/x(\equiv V_\infty/U_\infty)$. Three nonlinear results are illustrated. Solid blue lines depict disturbances excited using method **I**. For this particular problem, only the primary disturbance is excited. However, through nonlinear interaction its harmonics are stimulated and forced to grow proportionally with the primary mode. Dashed red and chain green lines depict simulation results driven by scheme **II** where positive c corresponds to blowing only and negative c suction, respectively. All Fourier modes are now excited equally, but the higher order harmonics are quickly forced to grow relative to the primary perturbation. The higher order harmonics would decrease in amplitude over the given range of x if not for the processes of nonlinear interaction. The magnitude of the linear only disturbance is included for illustration purposes and labeled using a black dotted line.
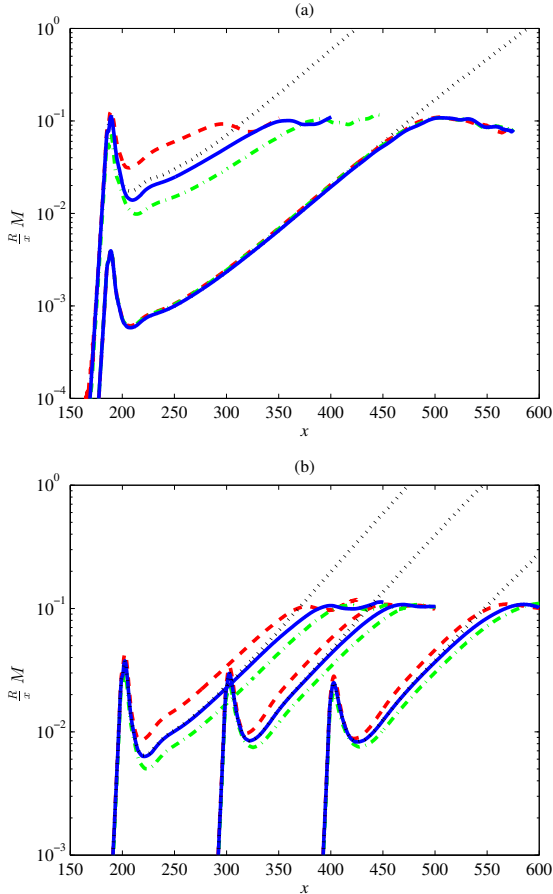
The first illustration (figure 2(a)) depicts the

Fig. 2 Maximum amplitudes of the primary Fourier u_1-velocity perturbation for forcing schemes $\{\mathbf{I}, c = 0.01\}$ (solid), $\{\mathbf{II}, c = 0.01\}$ (dashed) and $\{\mathbf{II}, c = -0.01\}$ (chain). The Reynolds number $R = 500$, the spanwise wavenumber $\beta = 0.4$ and centre of forcing $x_f = 186$. The dotted line represents the linear only result. (a): Extended chord range. (b): Localized about the centre of forcing.

effect of varying the forcing amplitude c on the receptivity of the disturbance. Two forcing amplitudes are considered: $c = 0.03$ in the upper half of the plot and $c = 0.001$ in the lower half. There are no discernible differences between the perturbation amplitudes generated using the smaller forcing (at least for $x < 400$). However, those disturbances excited by the larger amplitude of forcing display significant deviations from the linear only response.

The chord centre of the periodic forcing is varied in figure 2(b) to illustrate the effect of the disturbance distribution on the boundary-layer receptivity. The prescribed initial wall forcing magnitude $c = \pm 0.01$ is centred about the chord positions $x_f = 200$, 300 and 400. Method $\mathbf{I}$ has a marginal effect on the initial amplitude of the perturbation, whilst the disturbances driven by forcing scheme $\mathbf{II}$ again significantly augments (blowing - red dashed line) and reduces (suction - green chain line) the receptivity amplitude of the disturbance. As the centre of forcing x_f passes downstream along the chord direction, the perturbation amplitude decreases. This may be expected as it is well known that larger receptivity amplitudes are observed about neutrally stable conditions for crossflow [14, 15]. Thus, as x_f is increased to larger chord positions, differences between the responses of the three nonlinear perturbations are reduced. Further it is observed that all nonlinear perturbations attain a stationary point or as described here a state of equilibrium about an amplitude of 0.1.

The two methods of forcing have very different effects on the amplitude of the perturbation. Method $\mathbf{I}$ only causes small variations in the disturbance amplitude and it is only at larger chord locations that nonlinear modal interaction is relatively prominent. However, scheme $\mathbf{II}$ is found to have a significant effect on the amplitude of the disturbance response. This may not be too surprising as all four modes are initially excited and contribute towards the receptivity of the disturbance within the boundary-layer, whilst only the primary disturbance is activated through forcing scheme $\mathbf{I}$.

3.4 Receptivity Amplitudes

The formula for the receptivity amplitude A_c, equation (12), is applied to the perturbation results in figure 2(a) and solutions are plotted against the chordwise axis in figure 3(a). All line types are as before. The two dotted lines depict the receptivity amplitudes of the linear only perturbations. Downstream of the periodic forcing the linear receptivity amplitudes are constant over the chord length shown and their respective values are related through the size of the initial forcing c; $A_1 = 0.26$, $A_{0.03} = 0.0078$ and $A_{0.0001} = 0.00026$. Nonlinear receptivity amplitudes generated using the smaller initial forcing are almost identical over the chord length considered and only show significant changes to the linear result when $x > 400$. Downstream of this location the amplitude of the nonlinear disturbances are found to decrease rapidly.

The receptivity amplitudes given for the larger initial forcing are found to vary greatly. For instance, the receptivity amplitude generated by the wall blowing method **II** is initially almost double that given by the corresponding linear disturbance. However, as the crossflow disturbance evolves downstream its amplitude reduces in magnitude, eventually attaining values smaller than the linear solution. This behaviour is due to the nonlinear interaction of the primary Fourier mode with its higher order harmonics. (Note that results for the larger amplitude are cut off at $x = 400$ as this coincides with the onset of small-scale structures. The chosen chord grid size is too large to fully capture flow characteristics that develop following the emergence of nonlinear effects).

Repeating the calculations in figure 3(a) for values of $c \in [0.00001 : 0.05]$ and $x_f = 186$, the receptivity amplitudes depicted as four lines or curves in figure 3(b) are generated. Linear amplitudes are located along the straight black dotted line $A_c = 0.26c$. The corresponding nonlinear amplitudes are selected at the chord location $x = 250$. Results excited by scheme **II** are reflected about the linear line, with suction (green chain) having the expected stabilising effect on the receptivity amplitudes and blowing
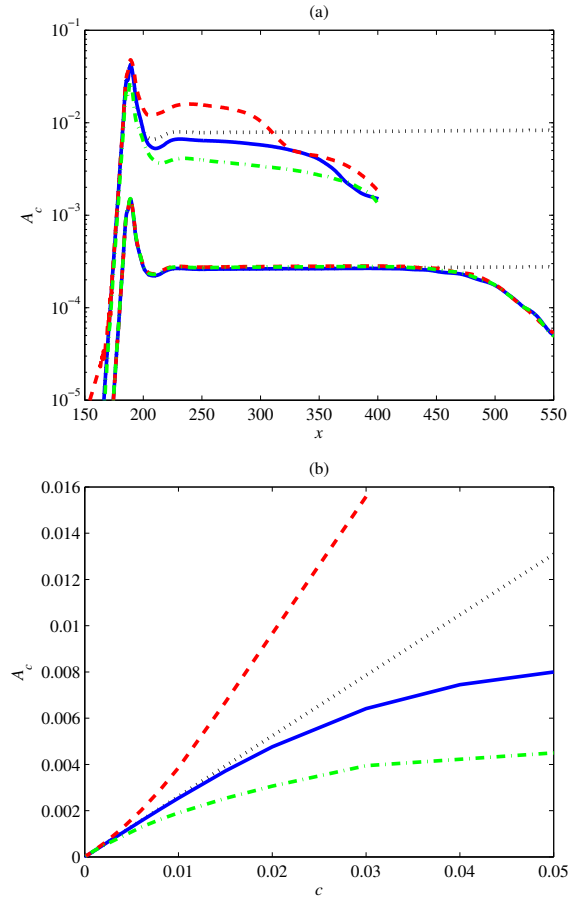

Fig. 3 (a): Receptivity amplitudes A_c plotted against chord length x. Line types correspond to that given in figure 8a. (b): Receptivity amplitudes A_c plotted against forcing magnitude $c \in [0.00001 : 0.05]$. Again line types match that given in figure 8.
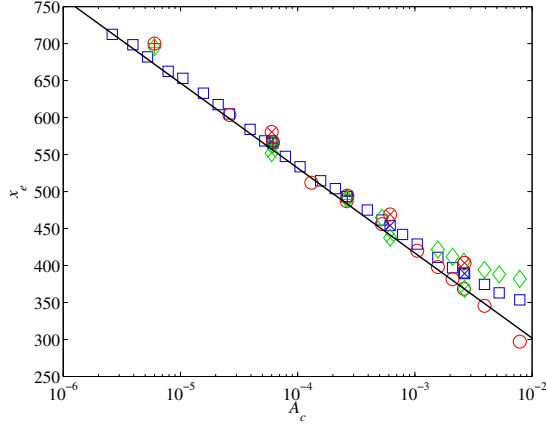
Fig. 4 The chord location that the primary disturbance attains a state of equilibrium (a value of 0.1 when normalised on R/x) plotted against the receptivity amplitude A_c of the <u>linear</u> disturbance.

(red dashed) destabilising. The third nonlinear curve (method **I** - blue solid) also shows a marked drop in the receptivity amplitude as c increases, though not to the extent illustrated by the suction only case.

3.5 Equilibrium Location

For all disturbances investigated, the maximum amplitude M, when normalised on R/x, attains a stationary point,

$$\frac{dM}{dx} = 0,$$

or a state of equilibrium about a magnitude of 0.1. Thus, we attempt to derive a relationship relating the equilibrium position x_e with one or more flow characteristics. The equilibrium locations x_e are plotted against the linear receptivity amplitude A_c (taken from the solid black line in figure 3(b)) in figure 4, where colour types are as before. Open markers correspond to disturbances excited about $x_f = 186$, while symbols with a $\times$ and $+$ at the centre are associated with the wall forcing prescribed at $x_f = 200, 300$ and 400, with $c = 0.01$ and 0.001, respectively. A semi-log scale has been used along the horizontal axis to aid illustration of results. The solid line depicts the location that the corresponding normalised linear calculation attains an amplitude of

0.1. Interestingly all nonlinear results are located within a very small bandwidth along this solid line, including those generated using alternative forcing locations, initial amplitudes and methods. The plot suggests that for a linear receptivity amplitude $A_c < 10^{-3}$, the chord position for equilibrium is approximately located along the line given by the linear solution. As A_c is raised to larger values, the range of x_e increases quite significantly, with chord variations on the order of 100 for $A_c = 10^{-2}$. However, it may still be possible to give a crude approximation for the location of equilibrium using the linear only calculation. Moreover, the size of the velocity perturbation at equilibrium can be estimated using the solutions of the linear receptivity calculations.

4 Final Discussion

An investigation has been carried out on the effects of nonlinearity on the development and receptivity of crossflow in the swept Hiemenz flow. Disturbances are generated using periodic forcing along the spanwise direction, using either a suction/blowing strip or a band of periodic holes. Only four spanwise Fourier modes are used to generate the nonlinear flow characteristics, but the resulting crossflow vortex evolution qualitatively agrees with the depictions given in [5].

Receptivity is investigated for a variety of initial forcing amplitudes and distributions. Suction and blowing holes have a significant effect on the amplitude of the disturbance. The absolute maximum of the primary u_1-velocity perturbation is found to stop growing linearly and attain a stationary point or a state of equilibrium about an amplitude of 0.1. For linear receptivity amplitudes $A_c \leq 10^{-3}$ the location for equilibrium is linearly proportional (on a log scaling) with the receptivity amplitude given by the linear only analysis. It is hypothesised that nonlinear receptivity calculations generated by alternative forcing methods (such as surface roughness) will also lie about this linear log line. (Note we have not considered the effect of boundary-layer receptivity to roughness, but it is possible to implement by suitably modifying the conditions for no-slip). This would suggest that some nonlinear

flow dynamics of the crossflow vortex development can be predicted directly from a linear only receptivity investigation.

References

[1] Gregory N., Stuart J. T. and Walker W. S. On the stability of three-dimensional boundary layers with application to the flow due to a rotating disk. *Phil. Trans. R. Soc. Lond. A*, Vol. 248, pp 155–199, 1955.

[2] Gray W. E. The nature of the boundary layer at the nose of a swept back wing. Unpublished, Min. Aviation, London, 1952.

[3] Malik M. R. The Neutral Curve for Stationary Disturbances in Rotating-Disk Flow. *J. Fluid Mech.*, Vol. 164, pp 275–287, 1986.

[4] Kohama Y. Study on boundary layer transition of a rotating disk. *Acta Mechanica*, Vol. 50, pp 193–199, 1984.

[5] Malik M. R. and Li F. and Chang C. -L. Crossflow disturbances in three-dimensional boundary layers : nonlinear development, wave interaction and secondary instability. *J. Fluid Mech.*, Vol. 268, pp 1–36, 1994.

[6] Poll D. I. A. Some observations of the transition process on the wind wood face of a long yawed cylinder. *J. Fluid Mech.*, Vol. 150, pp 329–356, 1985.

[7] Kohama Y., Saric W. S. and Hoos J. A. A high frequency instability of crossflow vortices that leads to transition. Proc. Roy. Aero. Soc.: Boundary-Layer Transition and Control, 1991.

[8] Morkovin M. V. On the many faces of transition, In Viscous Drag Reduction, ed. C.S. Wells, New York: Plenum. pp 1–31, 2001.

[9] Saric W.S., Reed H.L. and Kerschen E. J. Boundary-layer receptivity to freestream disturbances. *Annu. Rev. Fluid Mech.*, Vol. 34, pp 291–319, 2002.

[10] Choudhari M. Boundary-layer receptivity due to distributed surface imperfections of a deterministic or random nature. *Theoret. Comput. Fluid Dyn.*, Vol. 4, pp 101–117, 1993.

[11] Crouch J. D. Receptivity of three-dimensional boundary layers. AIAA, Aerospace Sciences Meeting and Exhibit, 31 st, Reno, NV, 1993.

[12] Collis S. S. and Lele S. K. Receptivity to surface roughness near a swept leading edge. *J. Fluid Mech.*, Vol. 380, pp 141–168, 1999.

[13] Davies C. and Carpenter P. W. A novel velocity-vorticity formulation of theNavier-Stokes equations with applications to boundary layer disturbance evolution. *J. Comp. Phys.*, Vol. 172, pp 119–165, 2001.

[14] Streett C.L. Direct harmonic linear Navier-Stokes methods for efficient simulation of wave packets. *AIAA Paper*, pp 1998–0784, 1998.

[15] Mughal S. Advanced Transition Prediction and Development of Linearised Navier-Stokes Receptivity Methods, Validation and Application. EADS-IW ref: IW102175, 2012.

Copyright Statement